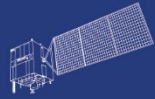


HY



HJ-1AB



CBERS



Gaofen



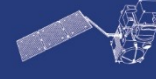
Beijing-2



Sentinel-1



Sentinel-2



Sentinel-3



Sentinel-5p



Aeolus

2023 DRAGON 5 SYMPOSIUM
3rd YEAR RESULTS REPORTING
11-15 SEPTEMBER 2023

[PROJECT ID. 59313]

**[GRASSLAND DEGRADATION DETECTION AND ASSESSMENT
BY REMOTE SENSING]**

<2023.9.14>

ID. 59313

**PROJECT TITLE: GRASSLAND DEGRADATION DETECTION AND ASSESSMENT
BY REMOTE SENSING**

PRINCIPAL INVESTIGATORS: ZHIHAI GAO & ALAN GRAINGER

CO-AUTHORS: BIN SUN, XIAOSONG LI, YIFU LI, ZIYU YAN, WEI YUE

PRESENTED BY: BIN SUN

Project's objectives

- (1) Mapping and dynamic monitoring of grassland types
- (2) Quantitative estimation of grassland ecological indicators
- (3) Degraded Grassland detection and assessment

LETTER

doi:10.1038/nature13376

Contribution of semi-arid ecosystems to interannual variability of the global carbon cycle

Benjamin Poulter^{1,2}, David Frank^{3,4}, Philippe Ciais², Ranga B. Myneni⁵, Niels Andela⁶, Jian Bi⁵, Gregoire Broquet², Josep G. Canadell⁷, Frederic Chevallier², Yi Y. Liu⁸, Steven W. Running⁹, Stephen Sitch¹⁰ & Guido R. van der Werf⁶

The land and ocean act as a sink for fossil-fuel emissions, thereby slowing the rise of atmospheric carbon dioxide concentrations¹. Although the uptake of carbon by oceanic and terrestrial processes has kept pace with accelerating carbon dioxide emissions until now, atmospheric carbon dioxide concentrations exhibit a large variability on interannual timescales², considered to be driven primarily by terrestrial ecosystem processes dominated by tropical rainforests³. We use

in order for us to be able to forecast long-term biospheric responses to climate change⁴.

High uncertainties in quantifying ecosystem processes mean that the global terrestrial carbon sink is often estimated as the residual between emissions from the combustion of fossil fuels, cement production and net land-use change, and sinks combining accumulation in the atmosphere and uptake by the ocean⁵. Using this method, the Global Carbon

Poulter B, et al. Nature, 2014.

CARBON CYCLE

The dominant role of semi-arid ecosystems in the trend and variability of the land CO₂ sink

Anders Ahlström^{1,2*}, Michael R. Raupach^{3†}, Guy Schurgers⁴, Benjamin Smith¹, Almut Arneth⁵, Martin Jung⁶, Markus Reichstein⁶, Josep G. Canadell⁷, Pierre Friedlingstein⁸, Atul K. Jain⁹, Etsushi Kato¹⁰, Benjamin Poulter¹¹, Stephen Sitch¹², Benjamin D. Stocker^{13,14}, Nicolas Viovy¹⁵, Ying Ping Wang¹⁶, Andy Wilshire¹⁷, Sonke Zaehle⁶, Ning Zeng¹⁸

The growth rate of atmospheric carbon dioxide (CO₂) concentrations since industrialization is characterized by large interannual variability, mostly resulting from variability in CO₂ uptake by terrestrial ecosystems (typically termed carbon sink). However, the contributions of regional ecosystems to that variability are not well known. Using an ensemble of ecosystem and land-surface models and an empirical observation-based product of global gross primary production, we show that the mean sink, trend, and interannual variability in CO₂ uptake by terrestrial ecosystems are dominated by distinct biogeographic regions. Whereas the mean sink is dominated by highly productive lands (mainly tropical forests), the trend and interannual variability of the sink are dominated by semi-arid ecosystems whose carbon balance is strongly associated with circulation-driven variations in both precipitation and temperature.

Since the 1990s, terrestrial ecosystems have... an imbalance between the uptake of CO₂ through

Ahlström A, et al. Science, 2015.

Data access (list all missions and issues if any). NB. in the tables please insert cumulative figures (since July 2020) for no. of scenes of high bit rate data (e.g. S1 100 scenes). If data delivery is low bit rate by ftp, insert “ftp”

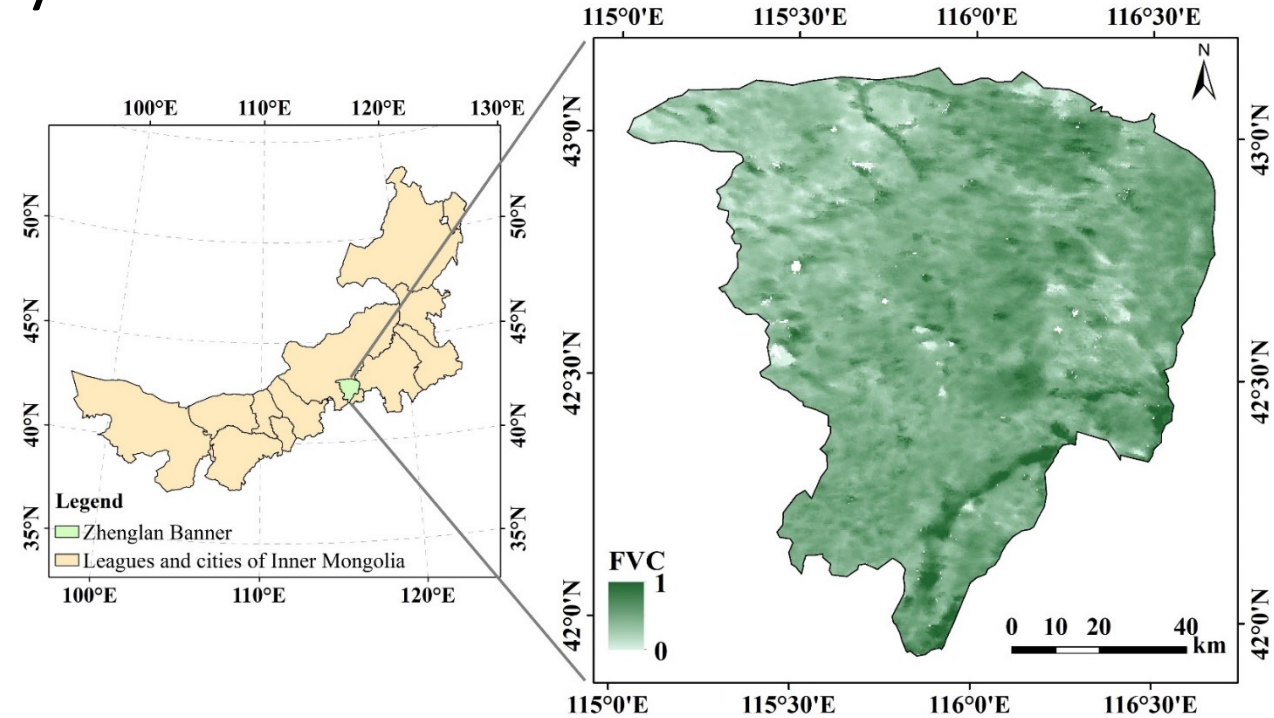
ESA /Copernicus Missions	No. Scenes	ESA Third Party Missions	No. Scenes	Chinese EO data	No. Scenes
1.S1	12	1. MODIS NDVI product	300	1.GF-6 WFV	10
2.S2	12	2.		2.GLASS NPP	Global
3.		3.		3.	
4.		4.		4.	
5.		5.		5.	
6.		6.		6.	
Total:		Total:		Total:	
Issues:		Issues:		Issues:	

Study area

Zhenglan Banner is situated in the southern part of XilinGol League in Inner Mongolia, within the Otindag sandy land hinterland. The region covers a total area of approximately 10,182 km².

Zhenglan Banner falls under the mid-temperate continental monsoon climate category, characterized by an average annual temperature of 1.5 °C and an average annual rainfall of 362.5 mm, mostly concentrated from June to September.

Herbaceous vegetation represents a valuable resource in Zhenglan Banner, with the available grassland area accounting for 86.88% of the total land area. Herbaceous vegetation types can be broadly classified into three main categories: meadow vegetation, typical grassland vegetation, and sand vegetation.



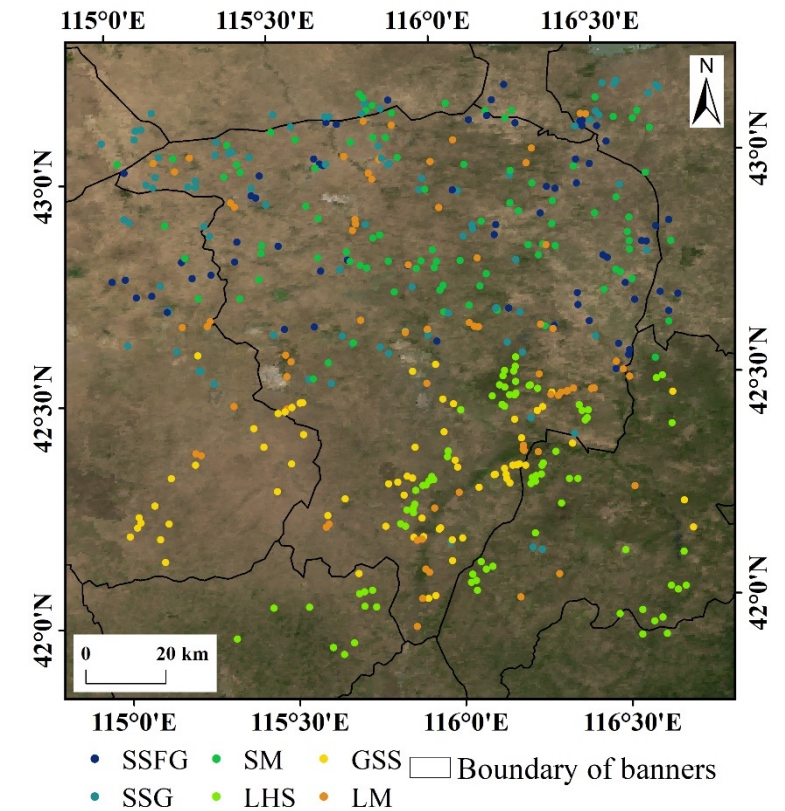
Being the nearest area of typical grassland and sand source to Beijing and Tianjin, Zhenglan Banner's ecological status holds significant importance. Many national initiatives focused on grassland protection and construction, resulting in substantial improvements in the regional ecological environment.

Detail the in-situ data measurements and requirements

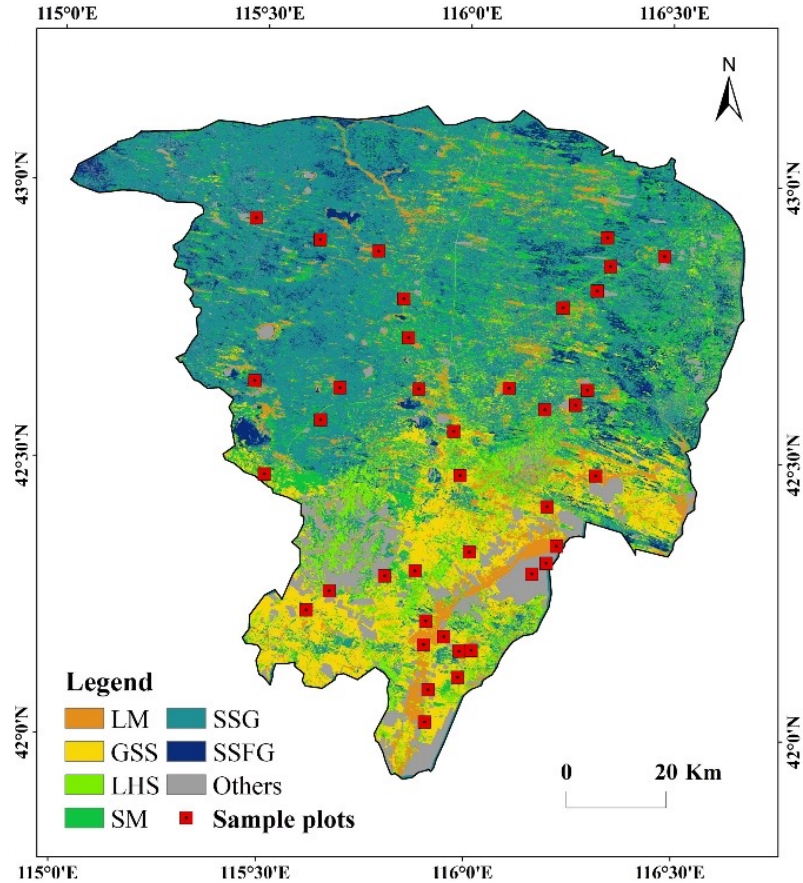
Sample Information for Grassland Type Classification

Grassland type	Number of classified samples	Number of validation samples	Total number of samples
Sandy sparse forest grassland	47	19	66
Sandy shrub grassland	61	26	87
Sandy meadow	63	27	90
Low hill steppe	57	24	81
gently sloping steppe	49	21	70
Lowland meadows	52	21	73

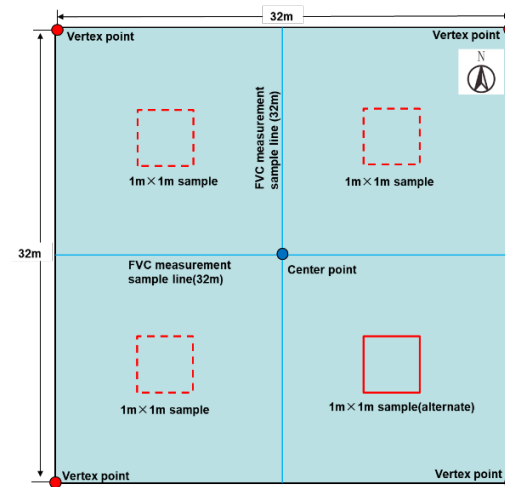
- Sample point data were obtained through field surveys conducted from August 10 to August 18, 2020, as well as visual interpretation of multitemporal GF-2 satellite multispectral data and submeter resolution images from Google Earth.
- A total of 467 sample points were collected, which were divided into training samples and validation samples in a 7:3 ratio.



Spatial distribution of samples for grassland classification



Distribution of center points of field-survey sample plots



Layout of sample plots and sampling method for aboveground biomass of grassland vegetation

25 grassland sample plots were set up in ZLQ

Sample plots was set to 32 m × 32 m square

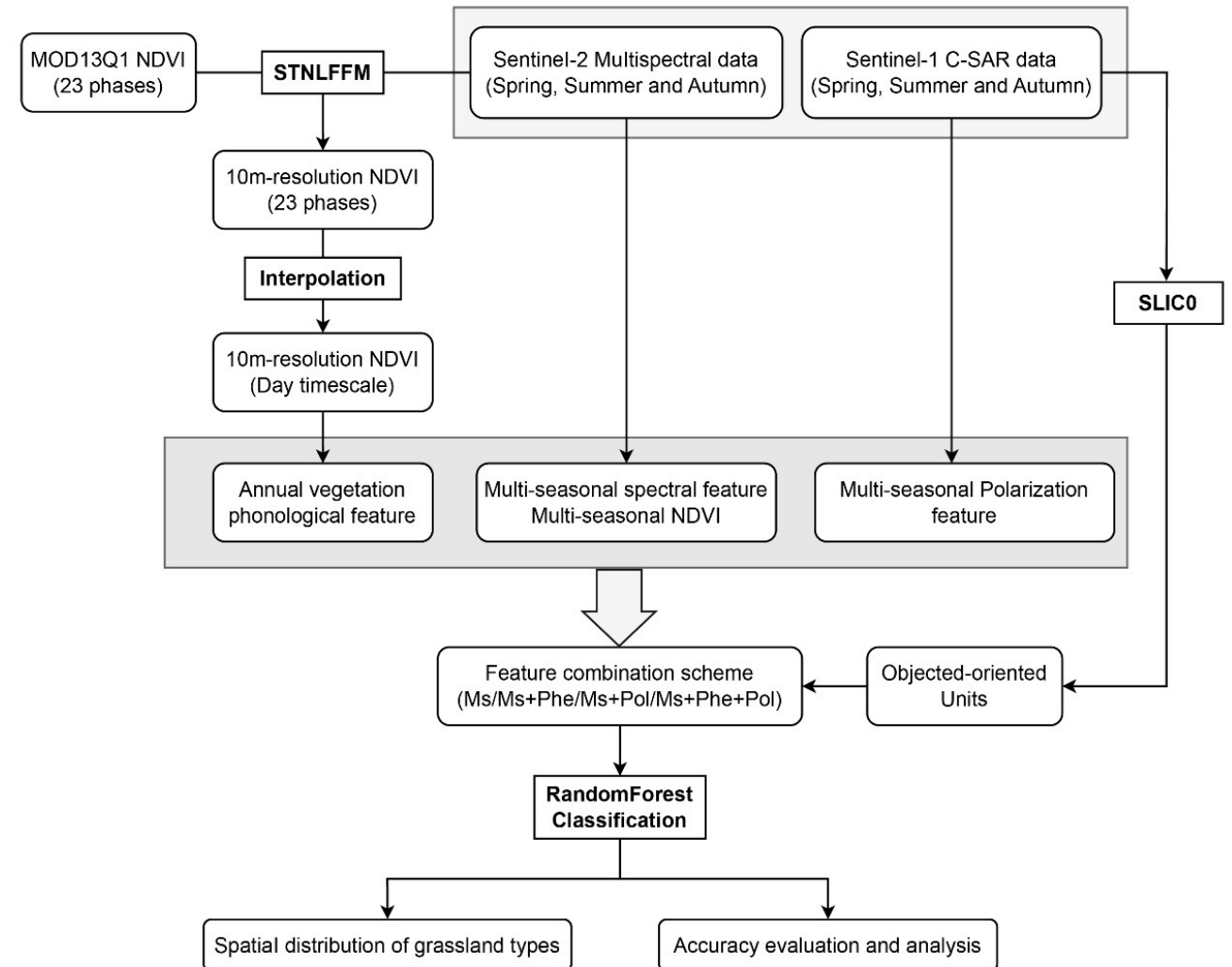
The aboveground parts from three 1 m × 1 m sample squares laid in each sample plot were harvested and placed into archive bags.

Vegetation coverage, grassland height, sample photographs, grassland type, and a description of the environment surrounding each sample plot were also recorded of the convenience of subsequent analysis and reference.

Integrating vegetation phenological characteristics and polarization features with object-oriented techniques for grassland type identification

- Due to the small size, variety, and high degree of mixing of herbaceous vegetation, remote sensing-based identification of grassland types primarily focuses on extracting major grassland categories, lacking detailed depiction.
- This limitation significantly hampers the development of effective evaluation and fine supervision for the rational utilization of grassland resources.
- To address this issue, it integrates the strengths of Sentinel-1 and Sentinel-2 active-passive synergistic observation and introduces innovative object-oriented techniques for grassland type classification, thereby enhancing the accuracy and refinement of grassland classification.



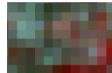

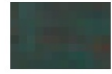







- (1) Acquisition of classification features, which includes extracting spectral features from multiseasonal Sentinel-2 MSI multispectral images, capturing polarization features from multiseasonal Sentinel-1 C-SAR data, and utilizing eight characteristic parameters representing the full cycle of vegetation growth.
- (2) Acquisition of geographic object units based on the SLIC0 superpixel algorithm.
- (3) Utilization of the random forest algorithm and characteristic data at the geographic object-level to identify grassland types, followed by verification of the classification accuracy using a confusion matrix.



Flow chart of grassland classification method

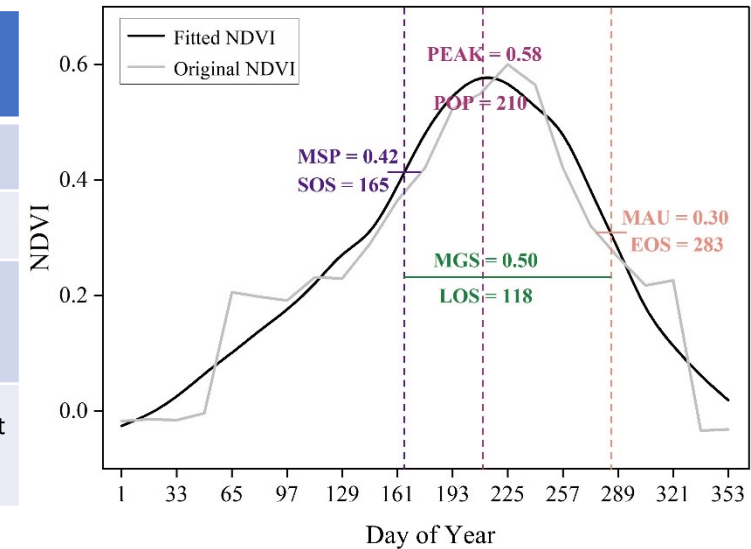
- Grassland remote sensing classification system

- Based on the aforementioned classification criteria for grassland types, and considering the suitability of medium spatial resolution remote sensing images and their practical applications in grassland management, this study adopts the vegetation-habitat classification method.
- Additionally, the research incorporates field survey data on grassland vegetation types in the study area and relevant data on livestock management. As a result, a relatively suitable grassland remote sensing classification system is developed.
- At the first level, the system primarily reflects soil texture, encompassing three grassland classes: sandy grassland, typical grassland, and meadow.
- At the second level, the system further delineates the heterogeneous characteristics within different grassland classes, consisting of six grassland subcategories: sandy sparse forest grassland, sandy shrub grassland, sandy meadow, low hill steppe, gently sloping steppe, and lowland meadow

Level 1	Level 2	Description	MSI image examples (Standard false color)	Sample plot photos
	Sandy sparse forest grassland	Elm sparsely forested landscapes with tree depression less than 0.3 and herbaceous cover greater than 5%. In the windward slopes of dunes and flat sandy areas, sandy pioneer plants such as <i>Agriophyllum squarrosum</i> ., <i>Salsola collina</i> Pall. and <i>Corispermum mongolicum</i> or <i>Artemisia intramongolica</i> H.C.Fu. are the main building blocks. The image tone is white and the texture is coarse.		
	sandy grassland	Shrubs are dominated by <i>Caragana microphylla</i> Lam. and herbs are mainly established by <i>Polygonum divaricatum</i> , <i>Artemisia intramongolica</i> H.C.Fu and <i>Agropyron mongolicum</i> , etc. The shrub cover is less than 30% and the herb cover is more than 5%. The image tone is greenish-gray with light red and rough texture.		
	sandy meadow	Located in the lowland between sand dunes, with no drifting sand disturbance on the surface, and crust layer developed, stable substrate, good soil moisture and nutrient status, mainly distributing communities such as <i>Stipa krylovii</i> Roshev., <i>Artemisia frigida</i> , <i>Agropyron cristatum</i> , <i>Zornia glochidiata</i> , <i>Leymus secalinus</i> , <i>Carex sp.</i> , etc., with herbaceous vegetation coverage more than 5%. The image tone is greenish-gray and uniform, the It is distributed in the low hills between 1250 and 1300 m above sea level. It is dominated by grass grasslands with poor weed species, and the representative establishment species are <i>Stipa krylovii</i> Roshev and <i>Artemisia frigida</i> . The total cover of the grassland is low. The image tone is greenish-gray, with clear boundaries with typical grasslands on gentle ground.		
	typical grassland			
	low hill steppe			
	gently sloping steppe	It is located on the high plains and in the peripheral areas of the mudflats, and is dominated by grassy grasslands with many mixed grasses, represented by <i>Zornia glochidiata</i> and <i>Stipa grandis</i> . Most of the grassland covers not less than 30%. The image tone is pink, with smooth and fine texture.		
	meadow			
	lowland meadow	It is found in saline lowlands on river floodplains, wide valley bottoms, inland lake basin margins, and poorly drained lowlands. The vegetation type is mainly mesophytic and wet mesophytic perennial herbaceous plants with dense grasses and little bare ground. The image tone is bright red but uneven, with smooth and fine texture.		

- Features for grassland types identification

Type	Variable name	Parameter	Definition or description
Spectral characteristics	Reflectance	B2~B4, B8	S2 MSI data for spring, summer, and autumn time phases
	Vegetation index	NDVI	$(B8-B4)/(B8+B4)$
Polarization characteristics	Backward scattering coefficient	σ	S1 C-SAR data in spring, summer, and autumn phases for two polarization modes VV and VH under σ
Phenological characteristics	Phenology	Phenological characteristics	SOS, EOS, LOS, POP, PEAK, MAU, MGS, MSP and other eight parameters



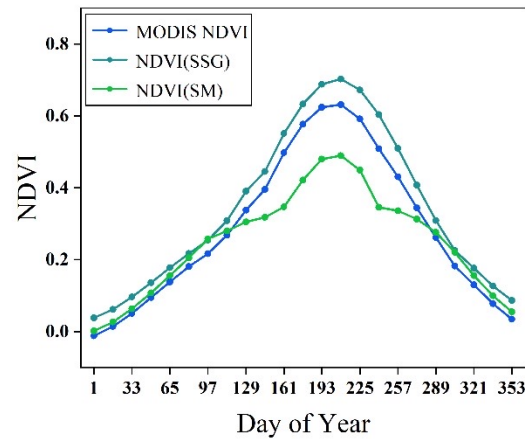
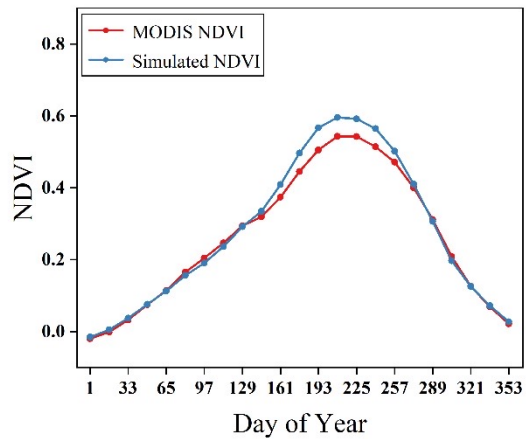
start of the season (SOS), end of the season (EOS), length of the season (LOS), position of peak value (POP), peak value (PEAK), mean autumn value (MAU), mean growing season value (MGS), and mean spring value

Phenological characteristics obtained using the extreme value method based on the first derivative of the NDVI time series

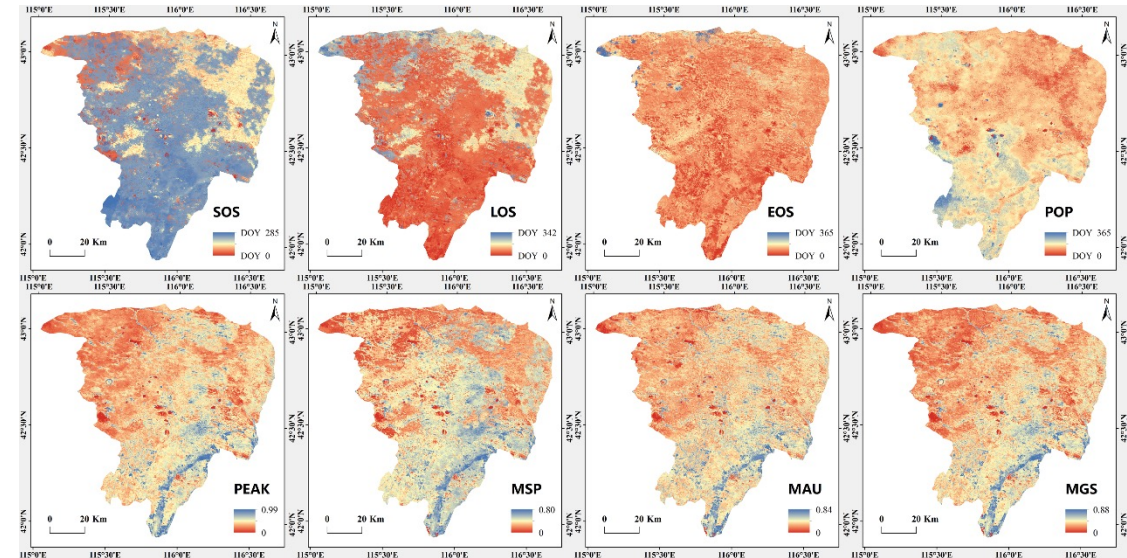
- Object-oriented classification

- Image segmentation: SLIC0 can adaptively select the optimal compactness parameter for each superpixel
- Classification: Random forest
- Classification accuracy evaluation: Production accuracy (PA), user accuracy (UA), overall accuracy (OA), and Kappa coefficient as metrics to summarize the classification performance.

Spatiotemporal fusion effect and phenological characteristic extraction



Comparison of fused NDVI time series with MODIS NDVI time series for pure pixel (a) and mixed pixel(b)

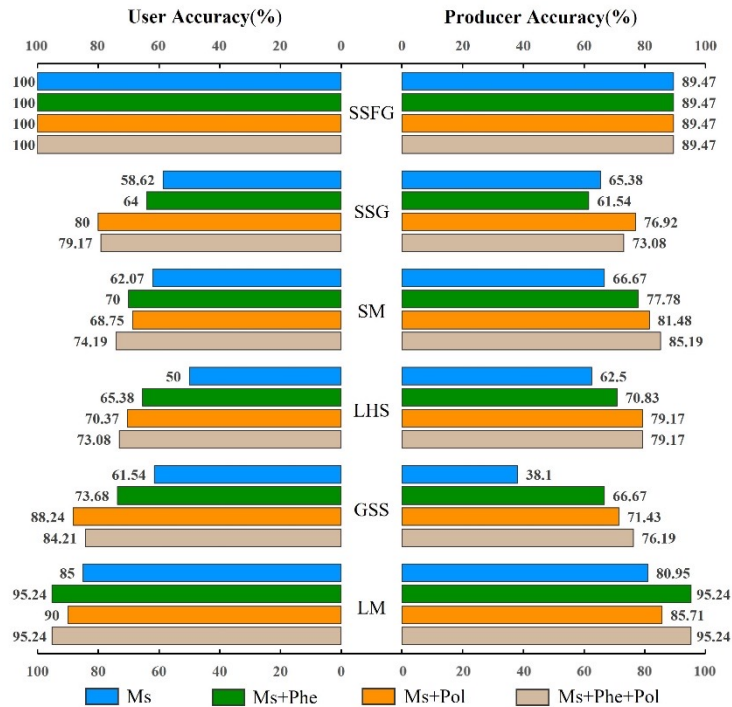


Eight phenological characteristics extracted based on the fused NDVI time series

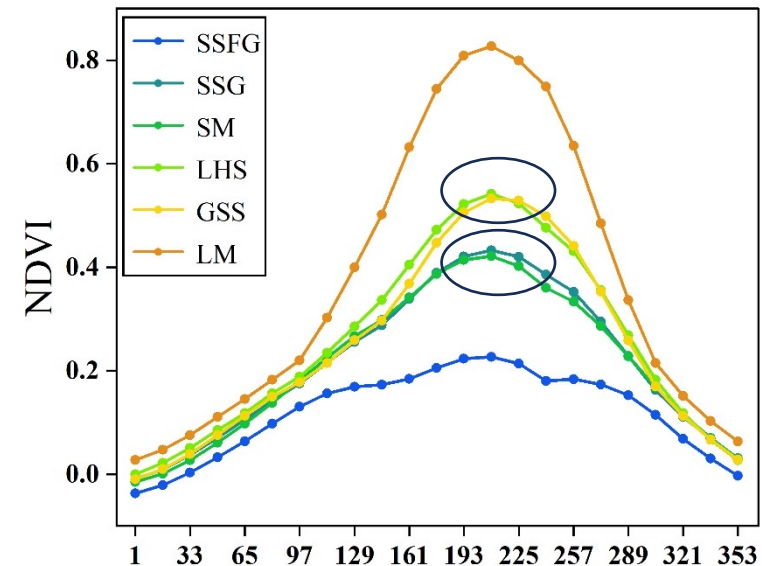
Influence of fusing different classification features on classification accuracy

Classification accuracy of different feature combinations

Combination method	Multiseasonal spectral	Multiseasonal spectral + Phenological	Multiseasonal spectral + Polarization	Multiseasonal spectral + Phenological + Polarization
OA (%)	66.67	76.09	80.43	82.61
Kappa coefficient	0.5975	0.7117	0.7639	0.7903

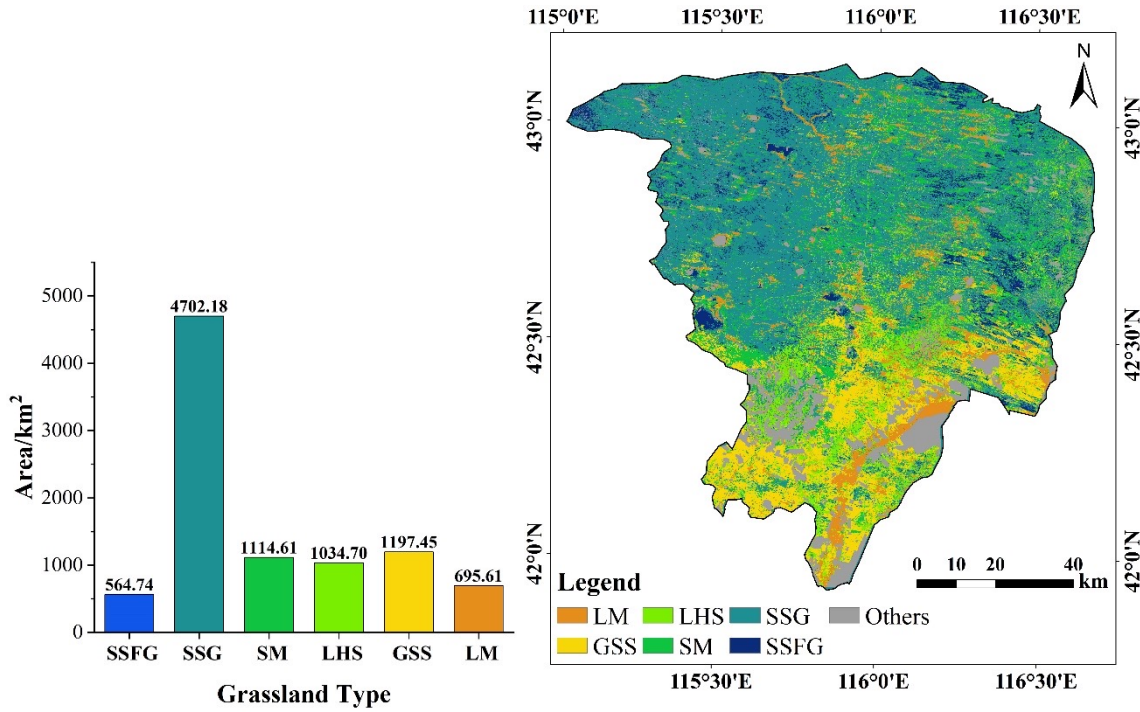


UA and PA of the six grassland types with different feature combinations

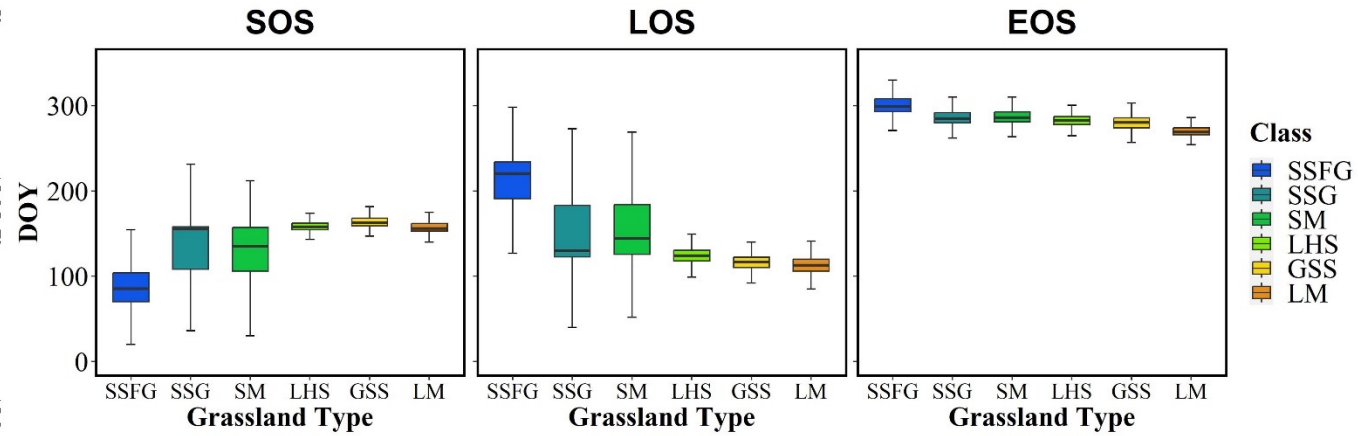


NDVI time series of six grassland types

Spatial distribution pattern of grassland types in Zhenglan Banner



Grassland type classification result in Zhenglan Banner



Box plots of phenological characteristics of different grassland types

Discussion

- (1) Construction of grassland remote sensing classification system
- (2) Use of remote sensing data
- (3) Application of remote sensing features for grassland type identification
- (4) Refinement of grassland type identification

Conclusions

(1) This study addresses the application needs of grassland resource regulation and proposes a grassland remote sensing classification system suitable for the northern natural grassland. This classification system can serve as a reference for constructing remote sensing fine identification systems for natural grasslands in other regions.

(2) This NDVI captures the temporal profile of grassland types and enables the accurate extraction of vegetation phenological information, particularly in mixed pixels. The method accurately reflects the changing characteristics of different grassland types at various growth stages, facilitating fine identification.

(3) Under the object-oriented framework, the study utilizes SLIC0 superpixel segmentation and random classification for the fine identification of grassland types. The classification method that integrates multiseasonal phase spectrum, polarization, and phenological characteristics achieves the highest classification effectiveness. The OA reaches 82.61%, with a Kappa coefficient of 0.79. The inclusion of separate polarization features and phenological characteristics enhances the classification accuracy by 13.76% and 9.42%, respectively.

High temporal and spatial estimation of grass yield by applying an improved Carnegie-Ames-Stanford Approach (CASA)-NPP transformation method

Grazing is the main and most important use of grasslands, and accurate estimation of the productivity of grassland with high temporal and spatial resolution is key to obtaining accurate evaluations of its livestock carrying capacity.

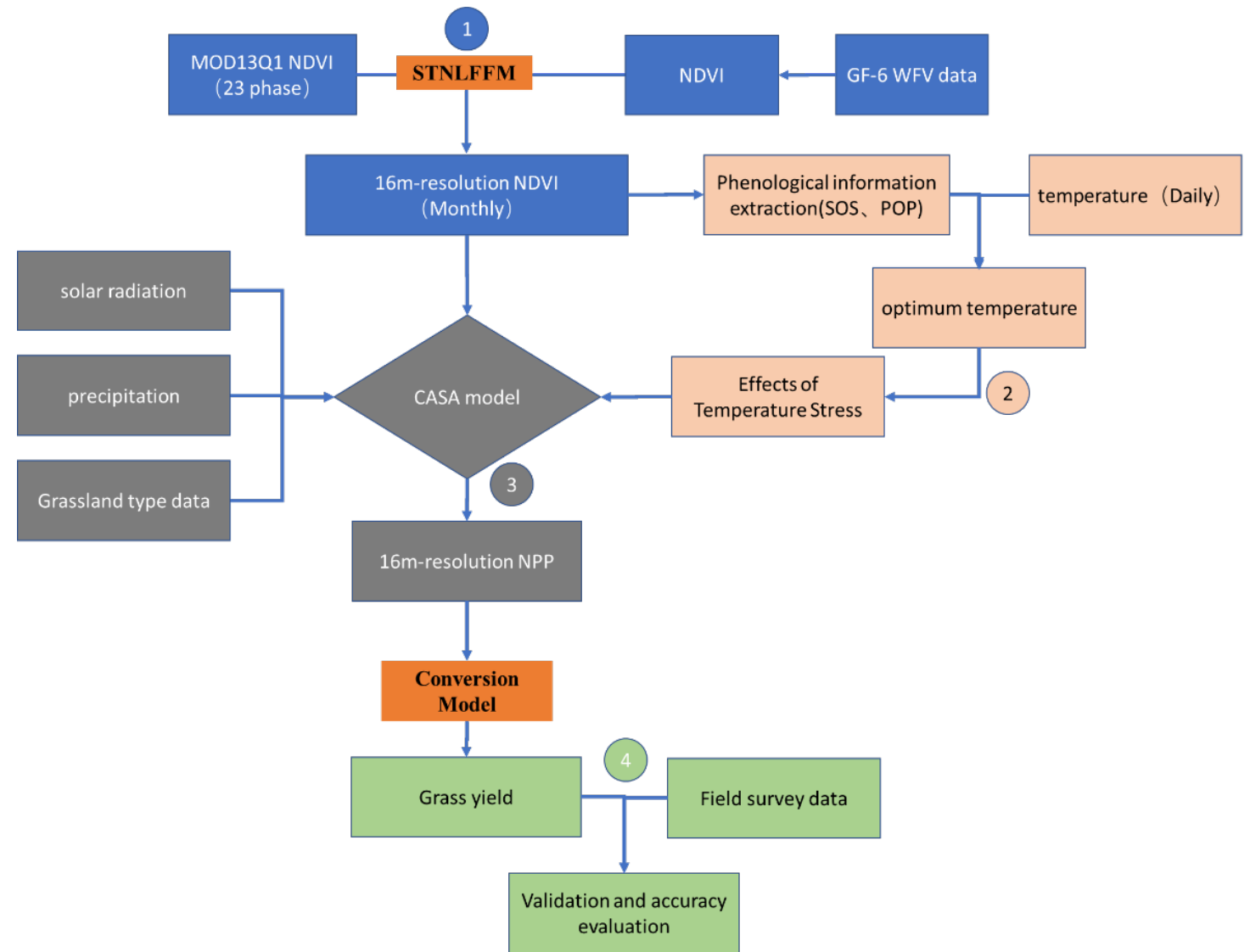
Methods for the estimation of grass yield based on remote sensing can be broadly classified into three categories: empirical methods, physical methods, and gross/net primary productivity (GPP/NPP) conversion methods, light-use efficiency (LUE) models are the most widely used for estimating grassland production

However, there are still uncertainties regarding some parameters and calculations in grass-yield estimations based on the CASA model. For example, the optimum temperature is an important parameter in the simulation of NPP, and it has a significant impact on the simulation effect.

This research had the following two objectives:

- (1) To study the reasonable expression of optimum temperature in the CASA model by combining the phenological performance characteristics of the grass-growth state across the whole cycle.
- (2) To construct an estimation model for grass yield with high temporal and spatial accuracy, and to analyze the applicability of the NPP conversion method for estimating the grass yields of different grassland types.

- Construction of high-temporal-resolution NDVI time-series datasets
- NPP estimation of grassland vegetation based on CASA model
- Construction of grass-yield estimation model based on NPP
- Validation



Flowchart of the research method

- Construction of high-temporal-resolution NDVI time-series datasets

$$F(x, y, t_p) = \sum_{k=1}^M \sum_{i=1}^N W(x_i, y_i, t_k) \times [a(x_i, y_i, \Delta t_k) \times F(x_i, y_i, t_k) + b(x_i, y_i, \Delta t_k)$$

- CASA model for NPP estimation

$$NPP(u, t) = APAR(u, t) \times \varepsilon(u, t),$$

$$APAR(u, t) = SOL(u, t) \times 0.5 \times FPAR(u, t),$$

$$\varepsilon(u, t) = T_{\varepsilon 1}(u, t) \times T_{\varepsilon 2}(u, t) \times W_{\varepsilon}(u, t) \times \varepsilon_{\max},$$

- Optimization of models based on optimum temperature

$$T_{\varepsilon 1}(u, t) = 0.8 + 0.02 \times T_{\text{opt}}(u) - 0.0005 \times (T_{\text{opt}}(u))^2,$$

$$T_{\varepsilon 2}(u, t) = \frac{1.184}{1 + e^{0.2 \times (T_{\text{opt}}(u) - 10 - T(x, t))}} \times \frac{1}{1 + e^{0.3 \times (-T_{\text{opt}}(u) - 10 + T(x, t))}},$$

- Construction of grass-yield estimation model based on NPP

$$GY = \frac{NPP}{C_{cf}} \times f_{\text{biomass}},$$

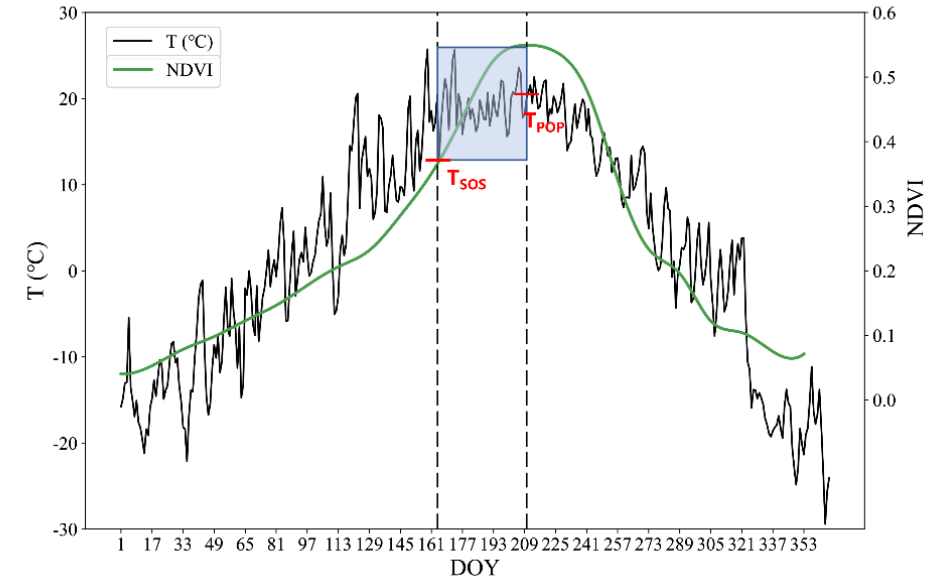
$$f_{\text{biomass}} = \frac{C}{C+1},$$

$$RRMSE = \frac{RMSE}{\text{Obs}} \times 100\%,$$

$$RMSE = \sqrt{\frac{\sum_{i=1}^n (\text{Obs}_i - \text{Est}_i)^2}{n}},$$

$$\text{Bias} = \frac{\sum_{i=1}^n (\text{Obs}_i - \text{Est}_i)}{n},$$

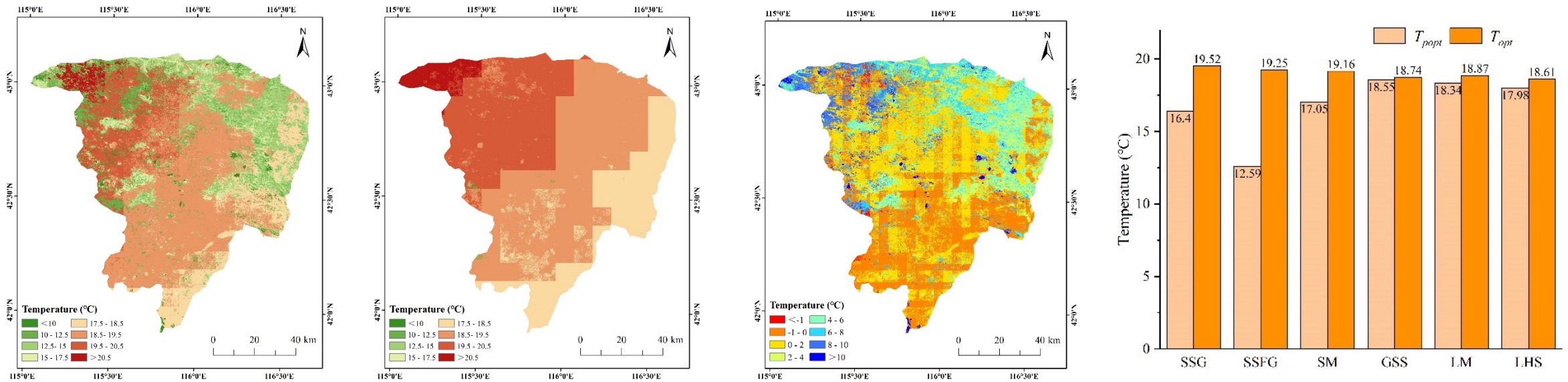
$$\delta = \frac{|\text{Est}_i - \text{Obs}_i|}{\text{Obs}_i} \times 100\%,$$



Intra-annual trends in grassland NDVI and temperature

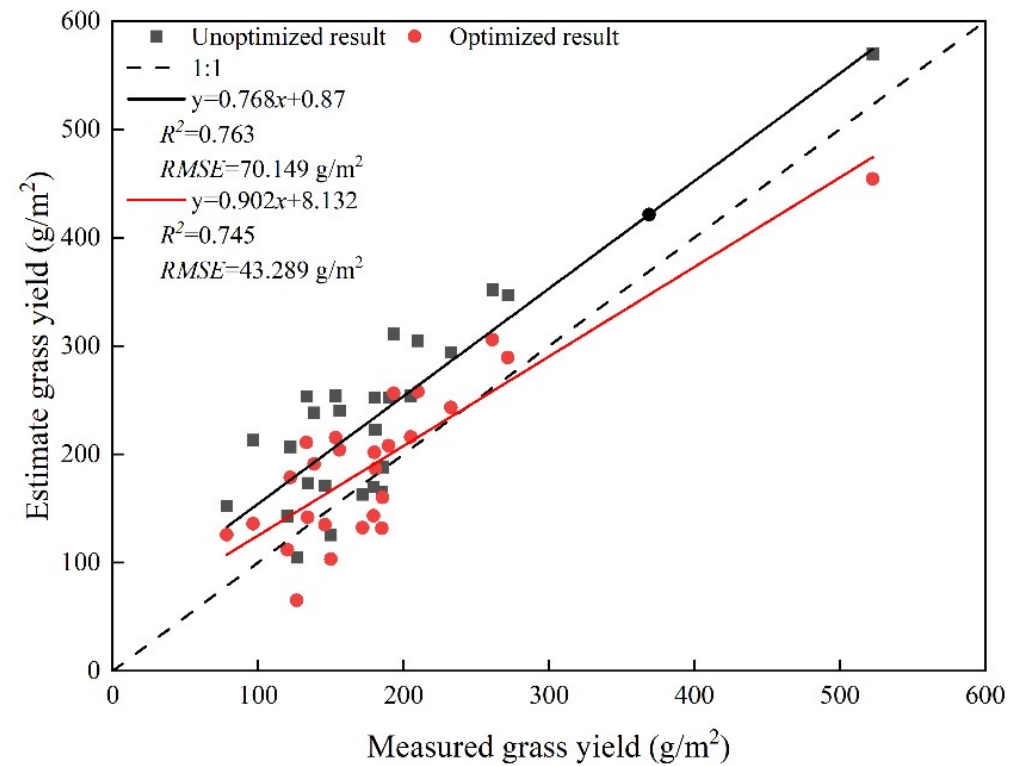
The SOS and POP parameters were determined by smoothing and interpolating the NDVI time series, testing their seasonality, and taking the extreme values of their first-order derivatives for the image elements with seasonality

Optimum temperature for grassland growth



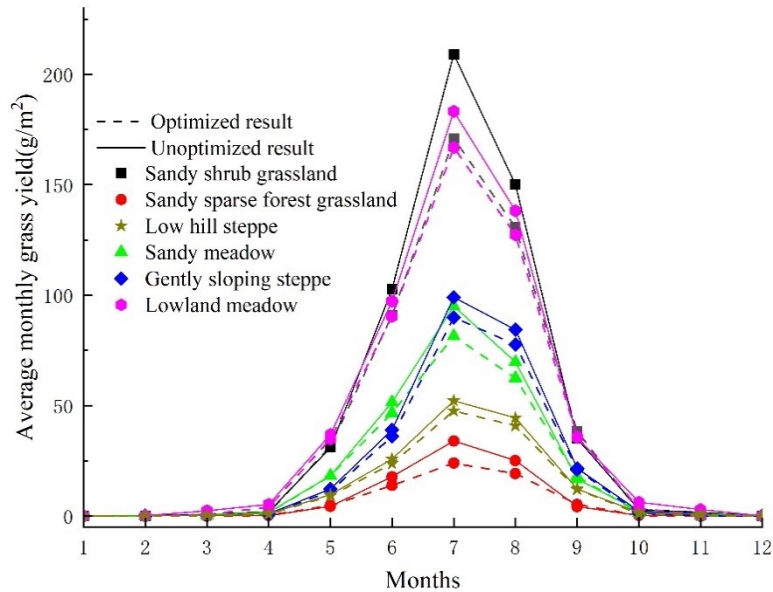
Spatial distribution of optimum temperature for vegetation growth defined by different methods in 2020 and the difference between T_{opt} and T_{popt}

Validation of the accuracy of the grass-yield estimation model



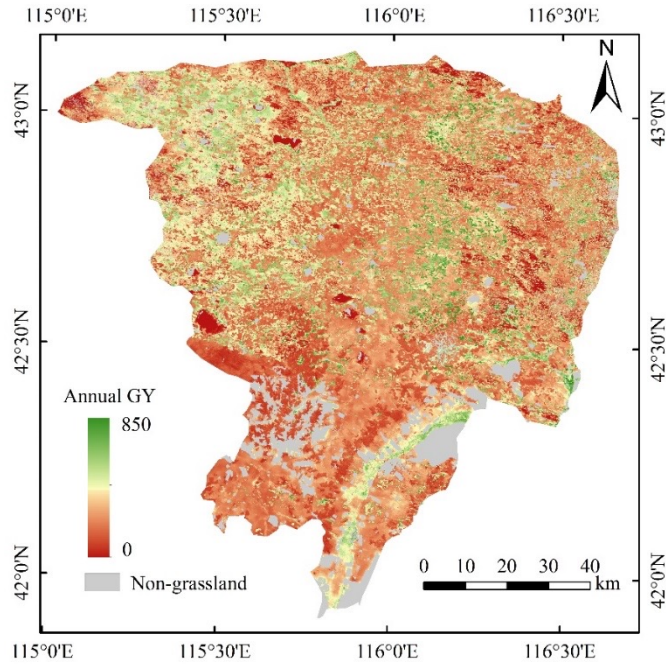
Comparison of the actual measured grass yields of the sample plots with the estimated results from the four grass-yield models

Temporal and spatial distribution characteristics of grass yield in Zhenglan Banner

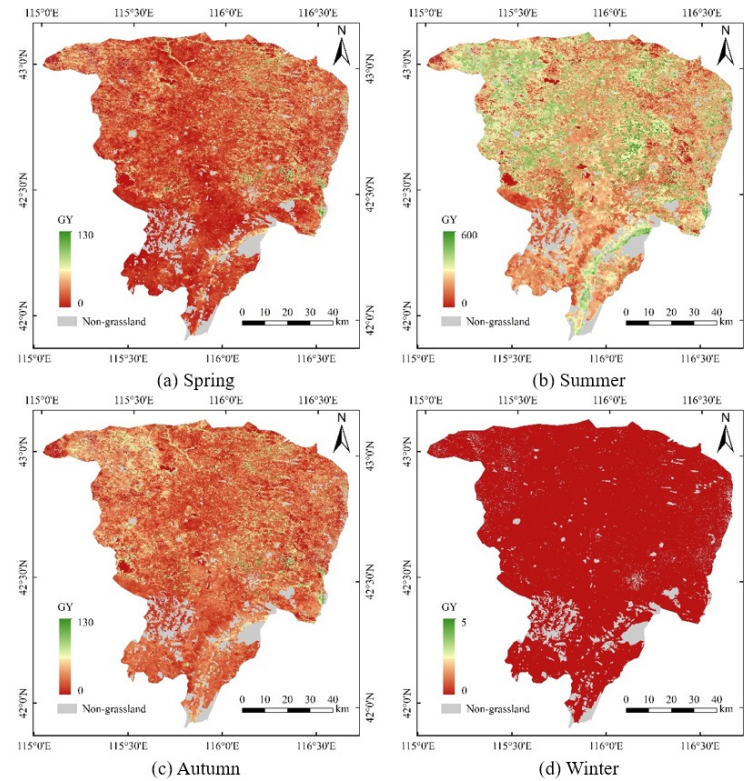


Grassland type	T_{popt} -based grass-yield model		T_{opt} -based grass-yield model	
	Grass yield (g/m ²)	Standard deviation (g/m ²)	Grass yield (g/m ²)	Standard deviation (g/m ²)
Sandy sparse forest grassland	86.08	7.76	67.49	7.00
Sandy shrub grassland	535.22	14.75	466.48	13.90
Sandy meadow	256.81	9.47	229.77	8.79
Low hill steppe	148.11	7.20	135.13	6.67
Gently sloping steppe	260.53	9.06	237.87	8.41
Lowland meadow	507.82	13.14	463.63	12.18

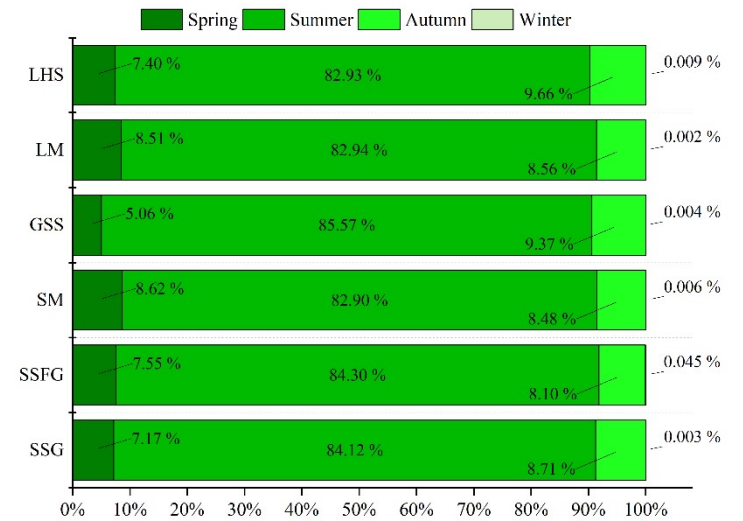
Time series of grass yields in different grassland types estimated by NDVIhi-based grass-yield model and NDVI_{mo}+T_{opt}-based grass-yield model



Spatial distribution of annual grass yield per unit area in grassland



Spatial distributions of seasonal grass yield per unit area in grassland



Intra-annual variations of the average grass yields of different grassland types

Discussion

- (1) Advantages and reliability of the method
- (2) Sources of estimation error
- (3) Association between grassland production and seasonal grazing

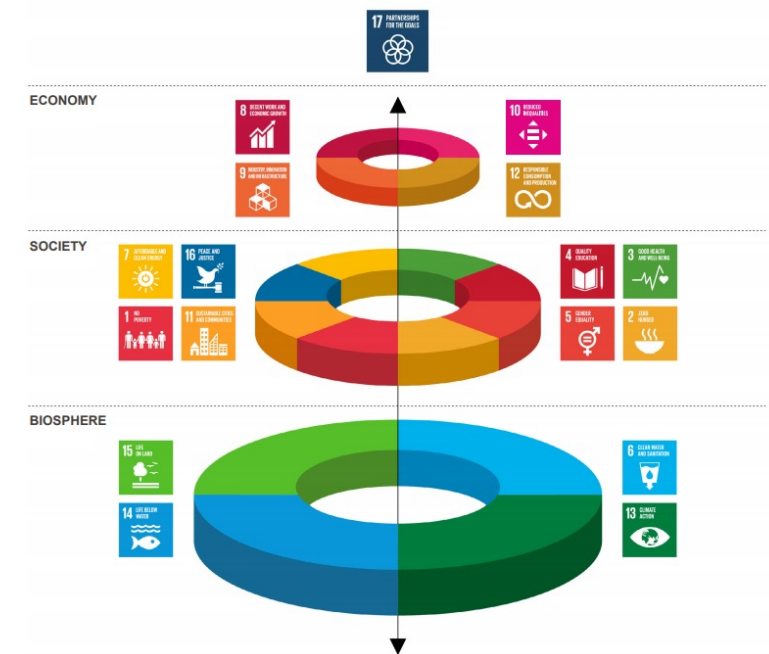
By fusing the advantages of the high spatial resolution and high temporal coverage of two sets of satellite data (GF-6 WFV data and MODIS data), an NDVI time-series dataset with high spatiotemporal resolution was generated. This achieved accurate extraction of grassland vegetation phenology information with high temporal and spatial resolution, and it thus allowed definition of the optimum temperature for vegetation growth from a phenology perspective, i.e., the period from the SOS to the period during which the NDVI maximum (the POP) is located. **This enhances the theoretical basis of the optimum temperature parameter in the model and minimizes the influence of anomalous NDVI maxima.** Compared with the original optimum temperature algorithm, the influence of the lag in grassland growth with respect to temperature is also largely solved.

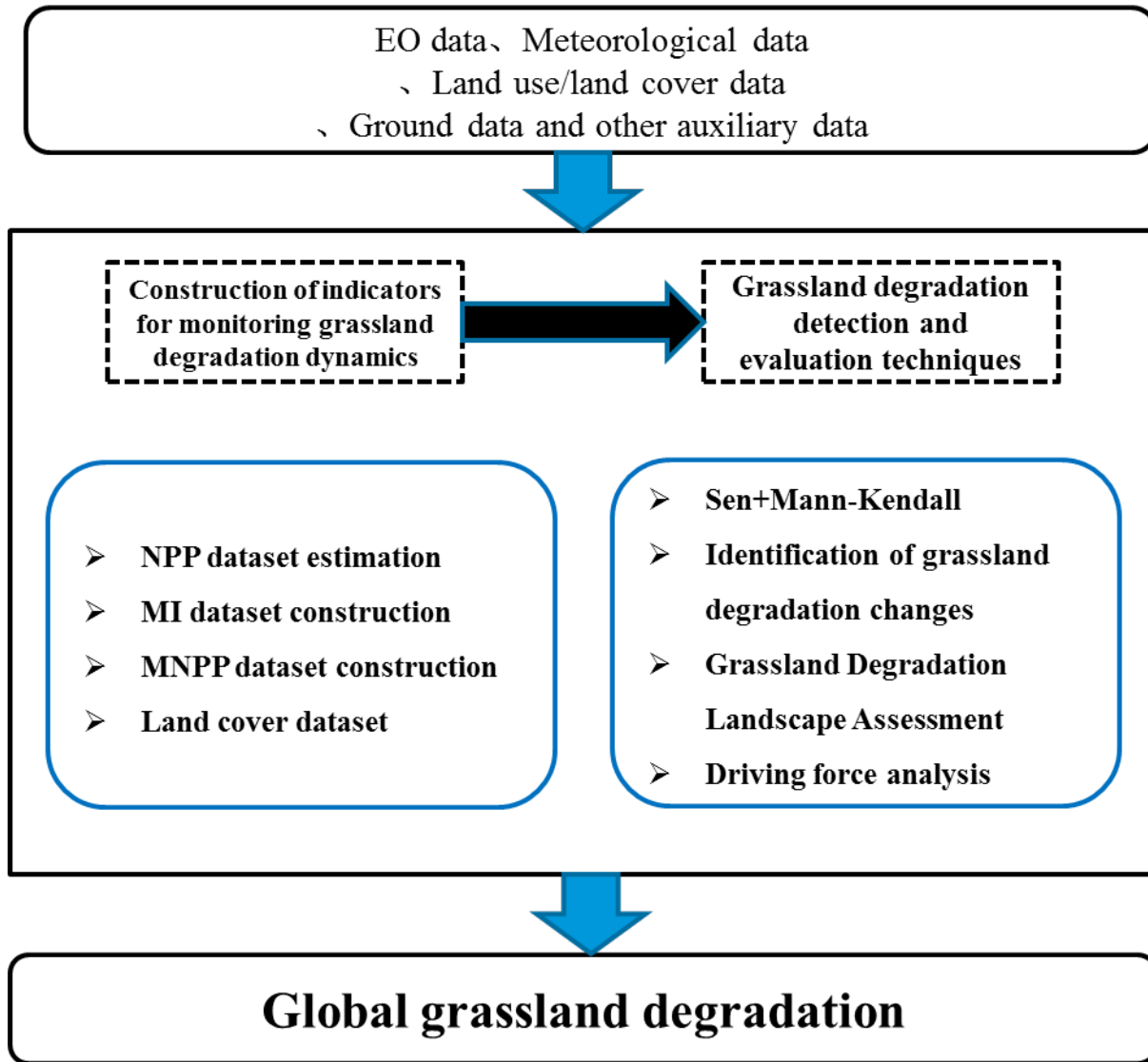
The correlation between NPP and the grass yield estimated based on the CASA model is very strong, and the correlation values between the models before and after optimization and the measured grass yield reached above 0.75 and were relatively close. The grass-yield model optimized by the optimum temperature was notably enhanced, and **the overall accuracy of the model's grass-yield estimation was improved by nearly 15 percentage points.** This was especially true in the sandy shrub grassland and lowland meadow, where the improvement effect was most obvious.

The total annual grass yield of Zhenglan Banner in 2020 based on this method was 2.94×10^{12} g, and the annual grass yield per unit area was 287.87 g/m². The basic characteristics of the spatial distribution of the yield were similar the distribution of grass types. **Due to differences in the main vegetation types of the different grasses, the seasonal grass yields of the different grassland types were somewhat different.** However, overall, they all accumulated mainly in summer, and growth in this season accounted for more than 80% of the annual grass yield.

Global Degradation Trends of Grassland and their Driving Factors Since 2000

- Grassland degradation threatens Sustainable Development Goals (SDGs) like poverty eradication, zero hunger, and climate action.
- There's a lack of standardized methods to assess global grassland degradation, hindering SDGs progress.
- Remote sensing and net primary production (NPP) offer effective tools to monitor and understand grassland degradation but require consistency and global applicability. Climate change impacts and benchmarking are key considerations.





Flowchart of the research method

● Calculation of the moisture-responded NPP (MNPP)

$$MNPP = \frac{NPP}{MI \times 100}$$

● Detection of areas of grassland degradation and improvement

$$\beta = \text{Median} \frac{x_j - x_i}{j - i} \quad (1 < j < i < n)$$

$$S = \sum_{i=1}^{n-1} \sum_{j=i+1}^n \text{sgn}(x_j - x_i)$$

$$Z = \begin{cases} \frac{S-1}{\sqrt{VAR(S)}} & S > 0 \\ 0 & S = 0 \\ \frac{S+1}{\sqrt{VAR(S)}} & S < 0 \end{cases}$$

$$\text{sgn}(x_j - x_i) = \begin{cases} 1 & \text{if } (x_j - x_i > 0) \\ 0 & \text{if } (x_j - x_i = 0) \\ -1 & \text{if } (x_j - x_i < 0) \end{cases}$$

$$VAR(S) = \frac{n(n+1)(2n+5) - \sum_{i=1}^m t_i(t_i-1)(2t_i-5)}{18}$$

● Quantitative identification of the driving factors

$$F_s = \frac{R^2_{NPP_1,2} - r^2_{NPP_2}}{(1 - R^2_{NPP_1,2}) / (n - 3)}$$

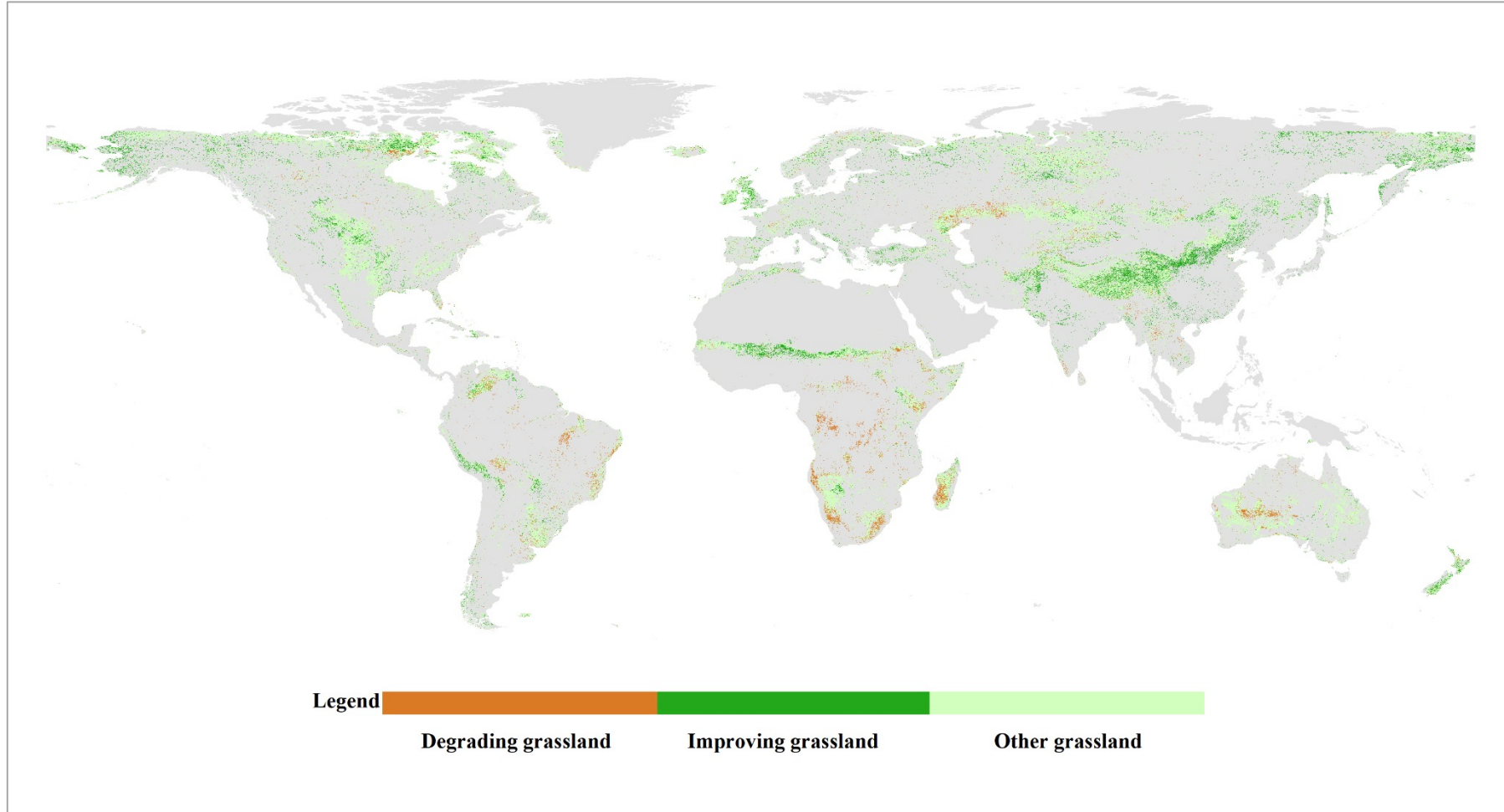
$$r_{12.3} = \frac{r_{12} - r_{13}r_{23}}{\sqrt{(1 - r^2_{13})(1 - r^2_{23})}} \quad t = \frac{r_{12.3} \times \sqrt{(n-k-2)}}{\sqrt{1 - r^2_{12.3}}}$$

- Standard for identifying trends in grassland degradation and improvement

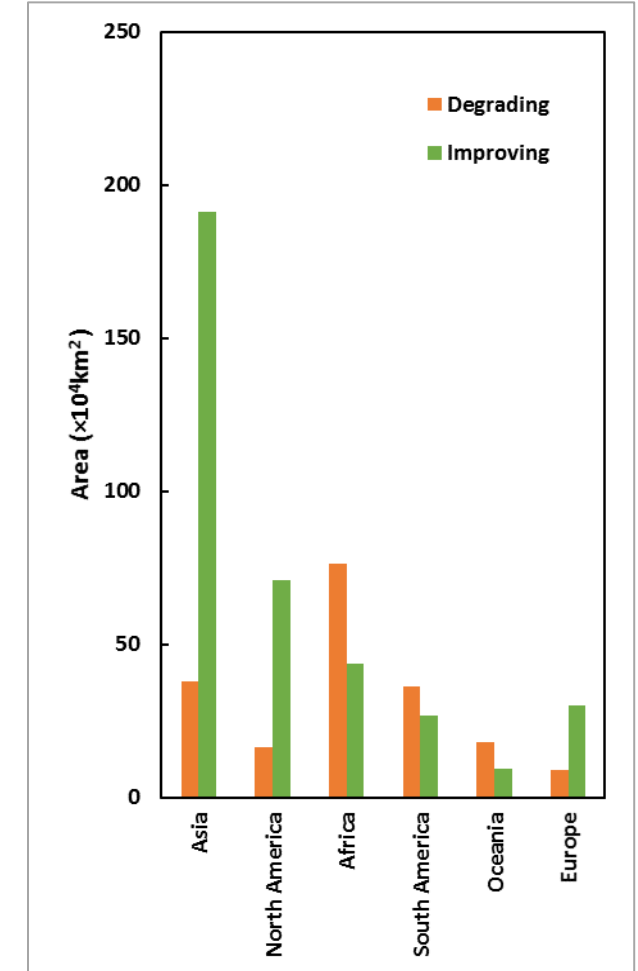
Indicators and change trend			NPP			
			Significantly decrease	Non-significant change	Significant increase	
MNPP	Significant increase	Significant negative correlation with MI	Degeneration	Fluctuation	Improvement	
		Other				
	Non-significant change			Improvement		
	Significantly decrease	Significant negative correlation with MI				Fluctuation
		Other				Fluctuation
						Degeneration

- Grassland degradation and improvement degree

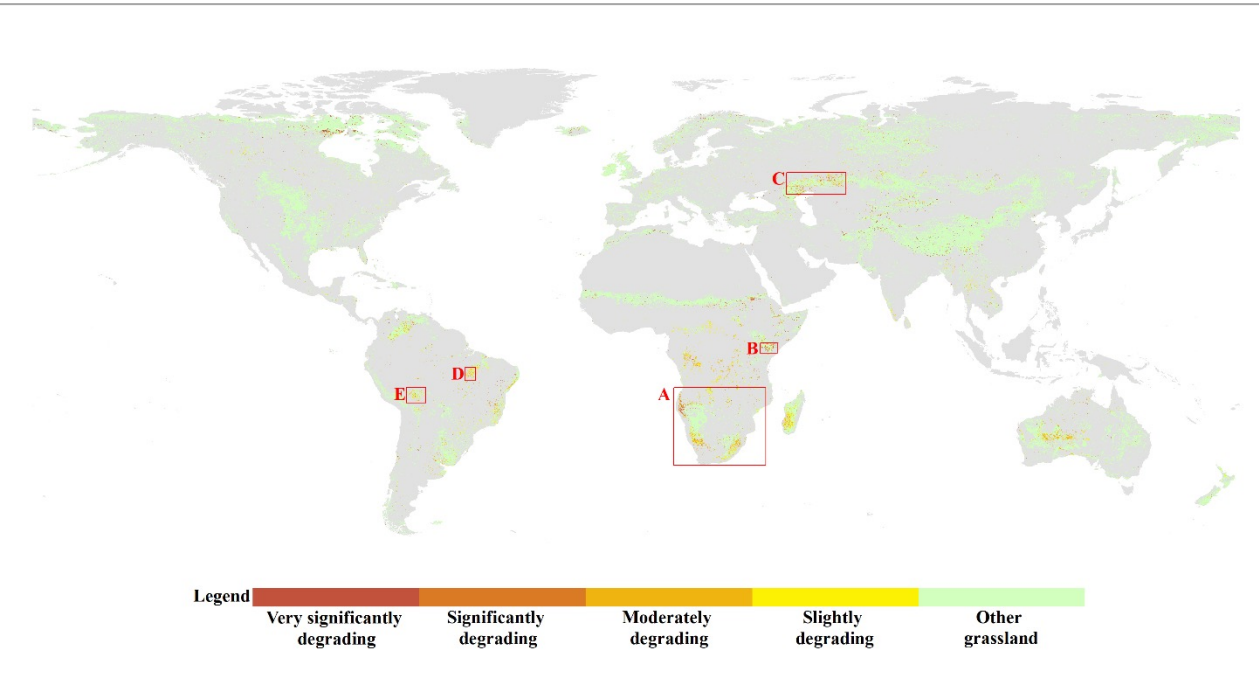
Categories	Degrees	Change rates (%)
Degrading	Very significantly degrading	<-30.0
	Significantly degrading	-30.0~-20.0
	Moderately degrading	-20.0~-10.0
	Slightly degrading	-10.0~0
Improving	Slightly improving	0~10.0
	Moderately improving	10.0~20.0
	Significantly improving	20.0~30.0
	Very significantly improving	>30.0



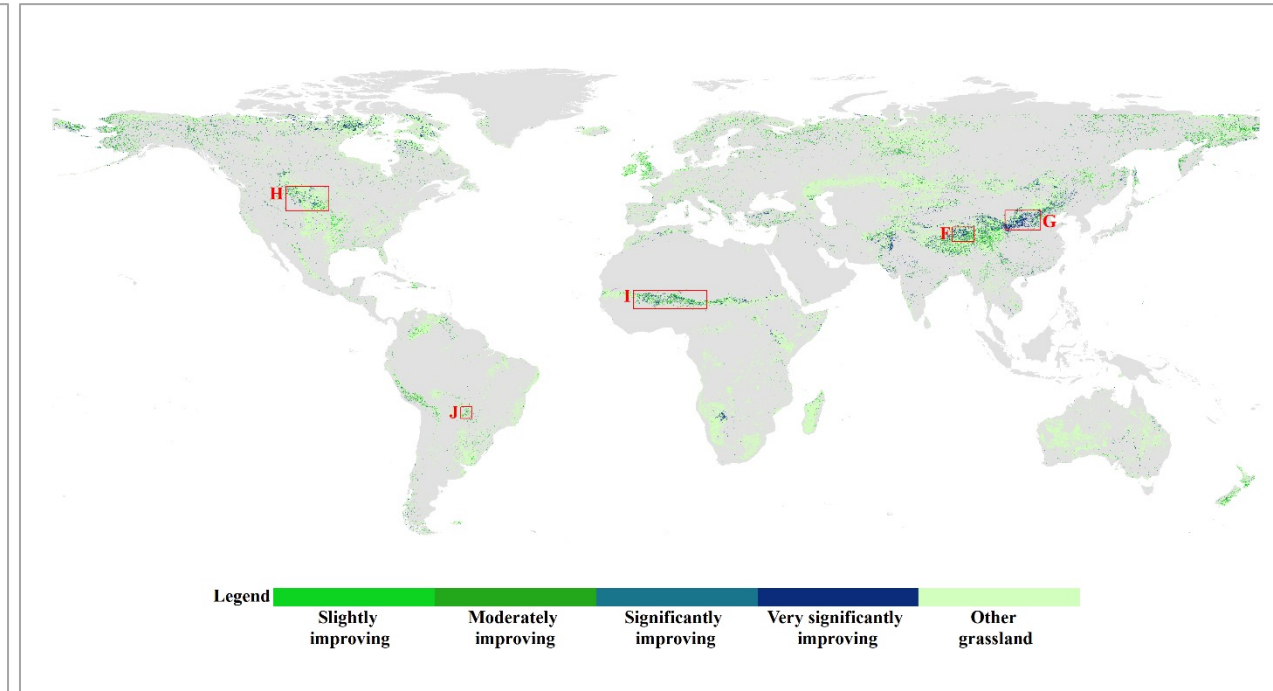
Distribution of global grassland degrading and improving areas from 2000-2020



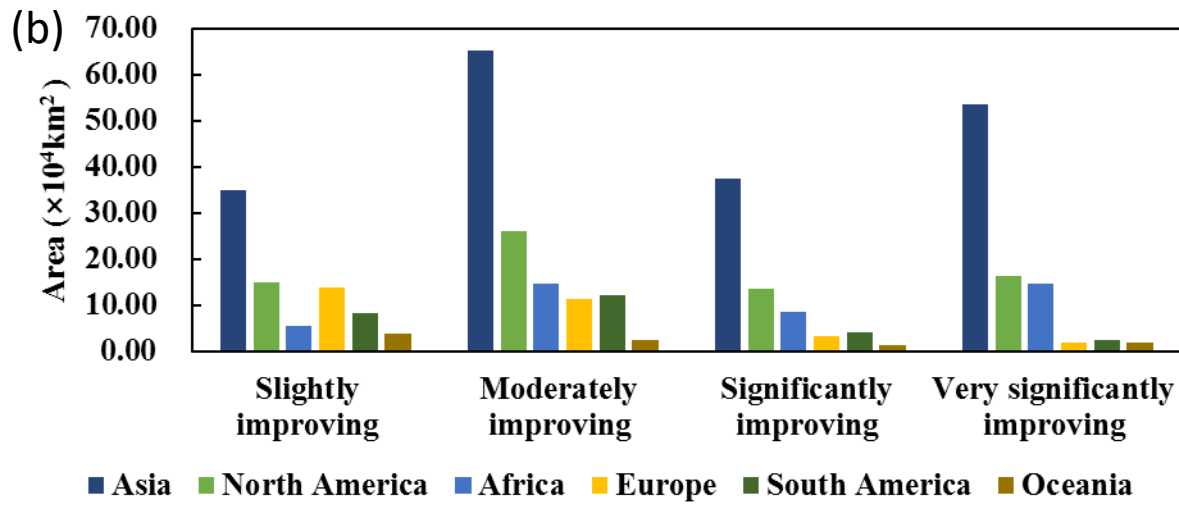
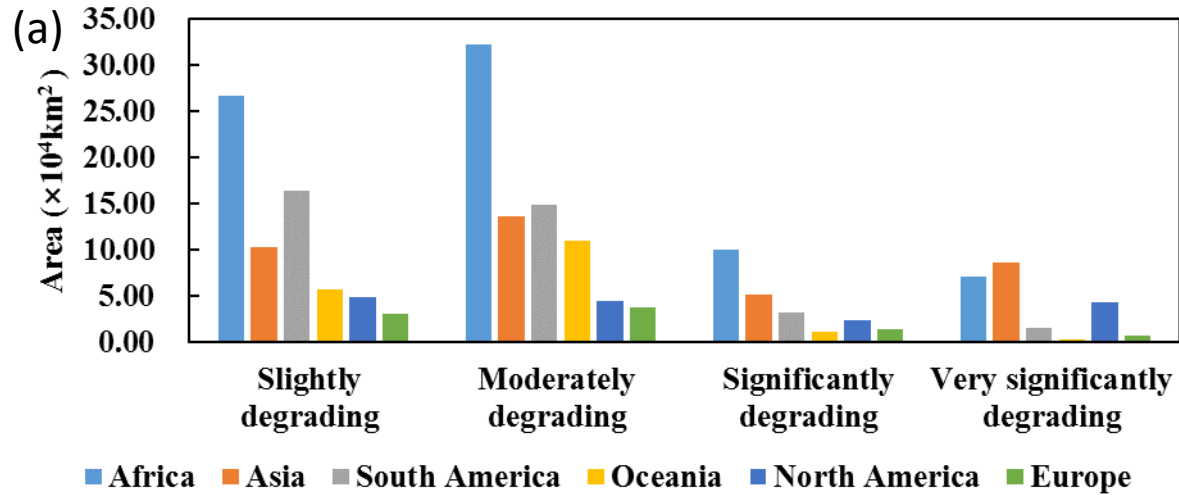
Area statistics by continent



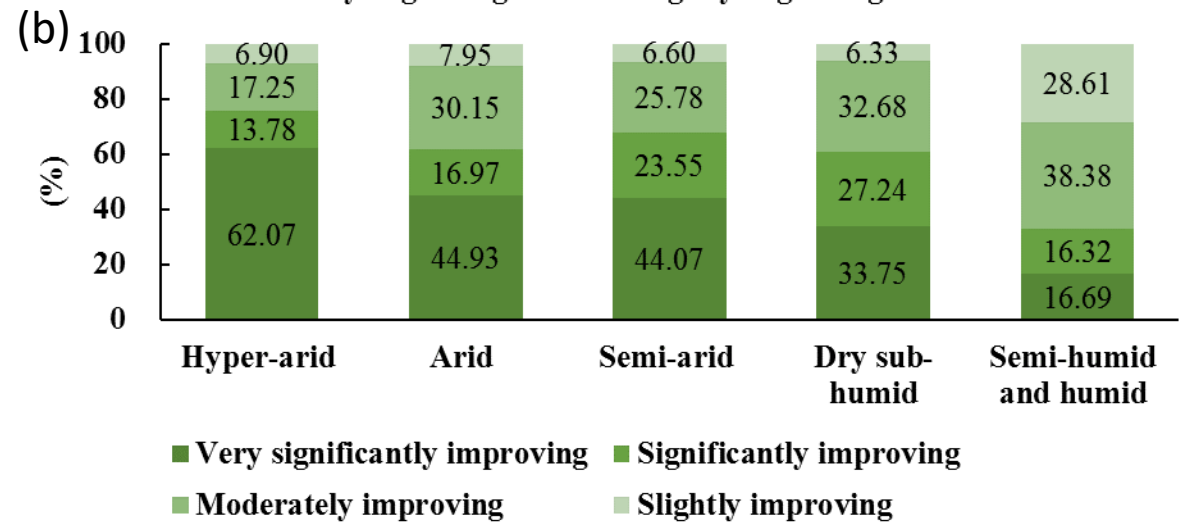
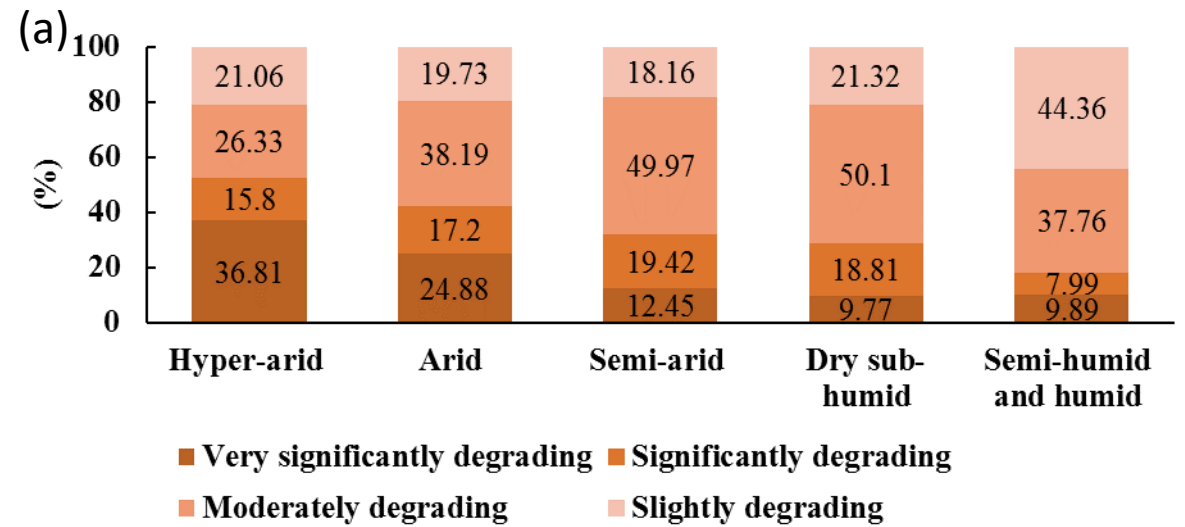
Distribution of global grassland degrading areas in different degrees from 2000-2020 and hotspots locations: Southern Africa (region A); East African Plateau (region B), Northern Asian Caspian (region C); Eastern Brazil plateau (region D); Northern Bolivia (region E)



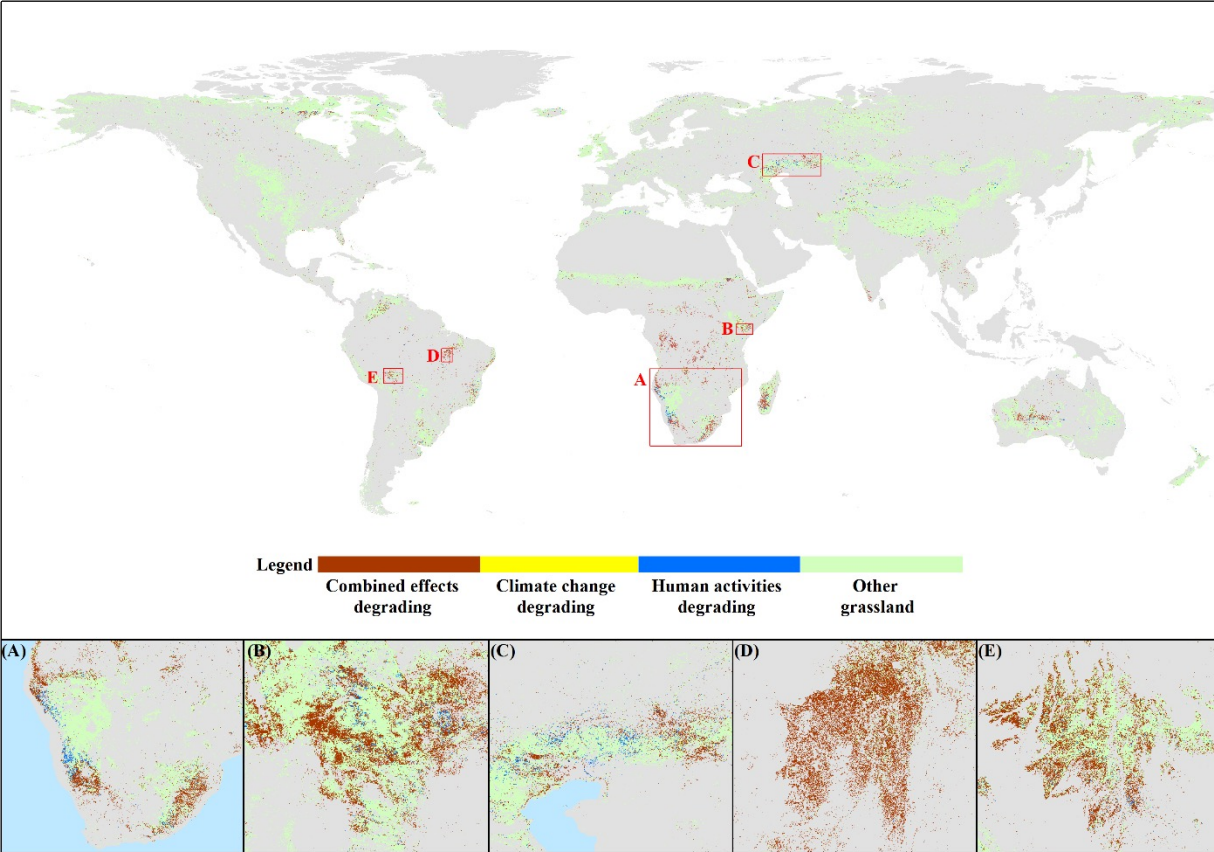
Distribution of global grassland improving areas in different degrees from 2000-2020 and hotspots locations: Qinghai-Tibet Plateau in China (region F), the Loess Plateau (region G), central North America (region H), and the western Sahel in Africa (region I); Northern La Plata (region J)



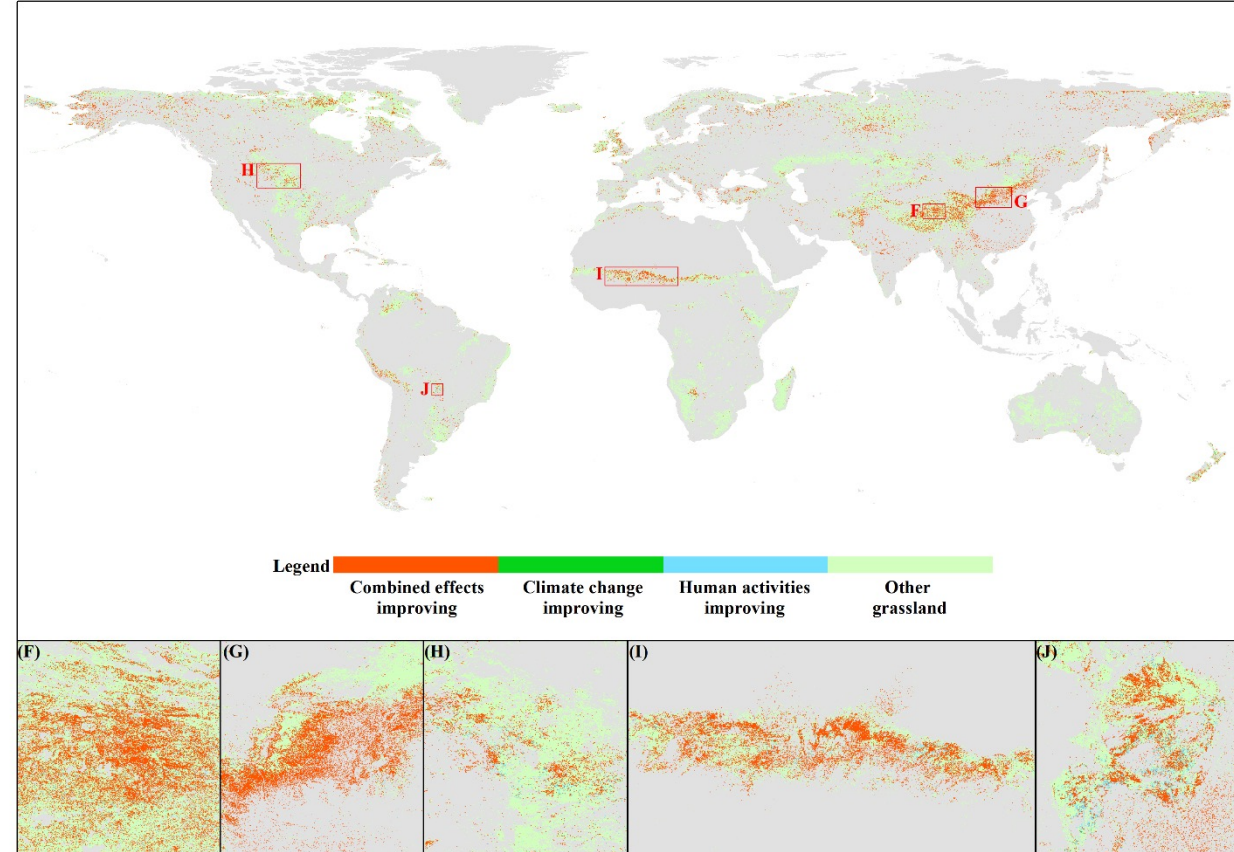
Global grassland degrading (a) and improving (b) to different degrees on each continent



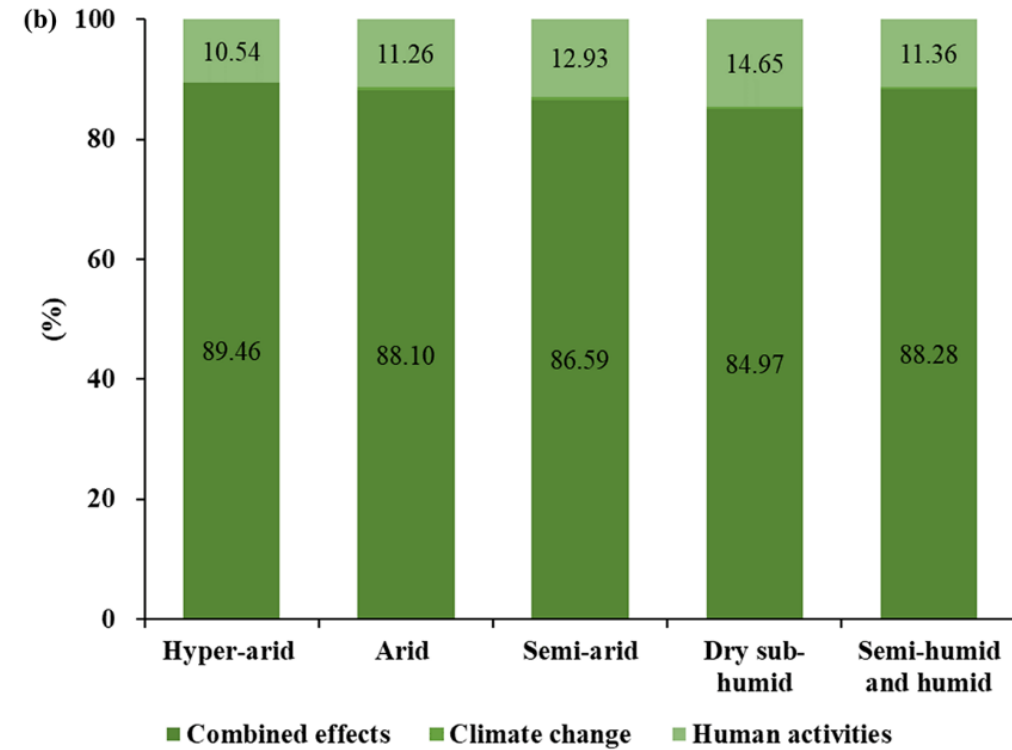
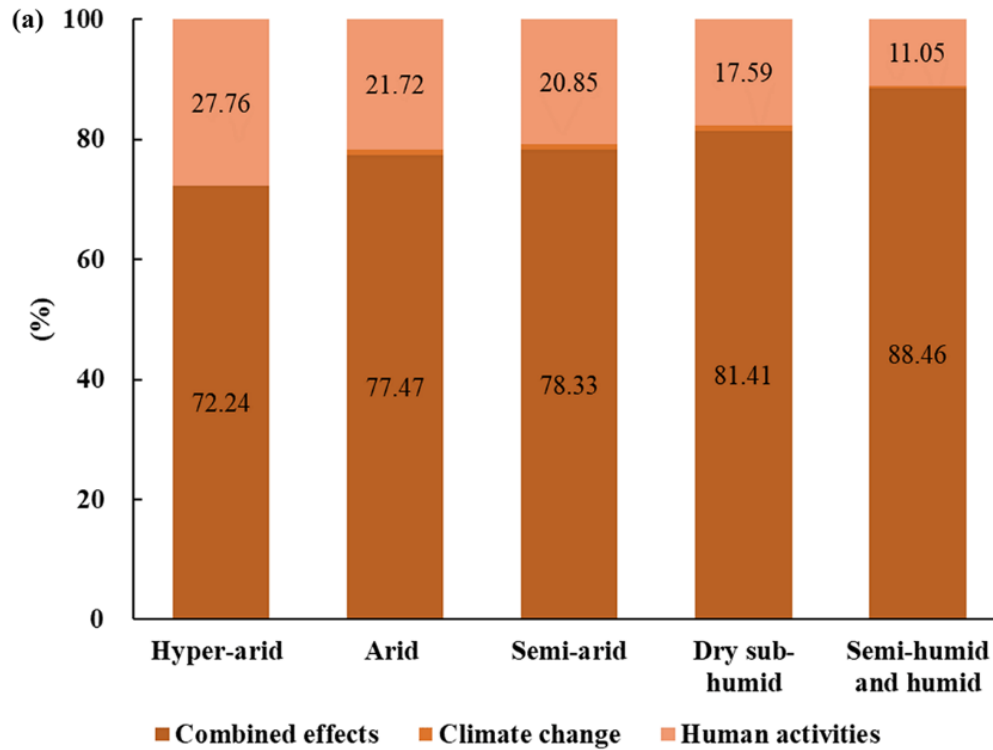
Global grassland degrading (a) and improving (b) proportion to different degrees in different climatic regions



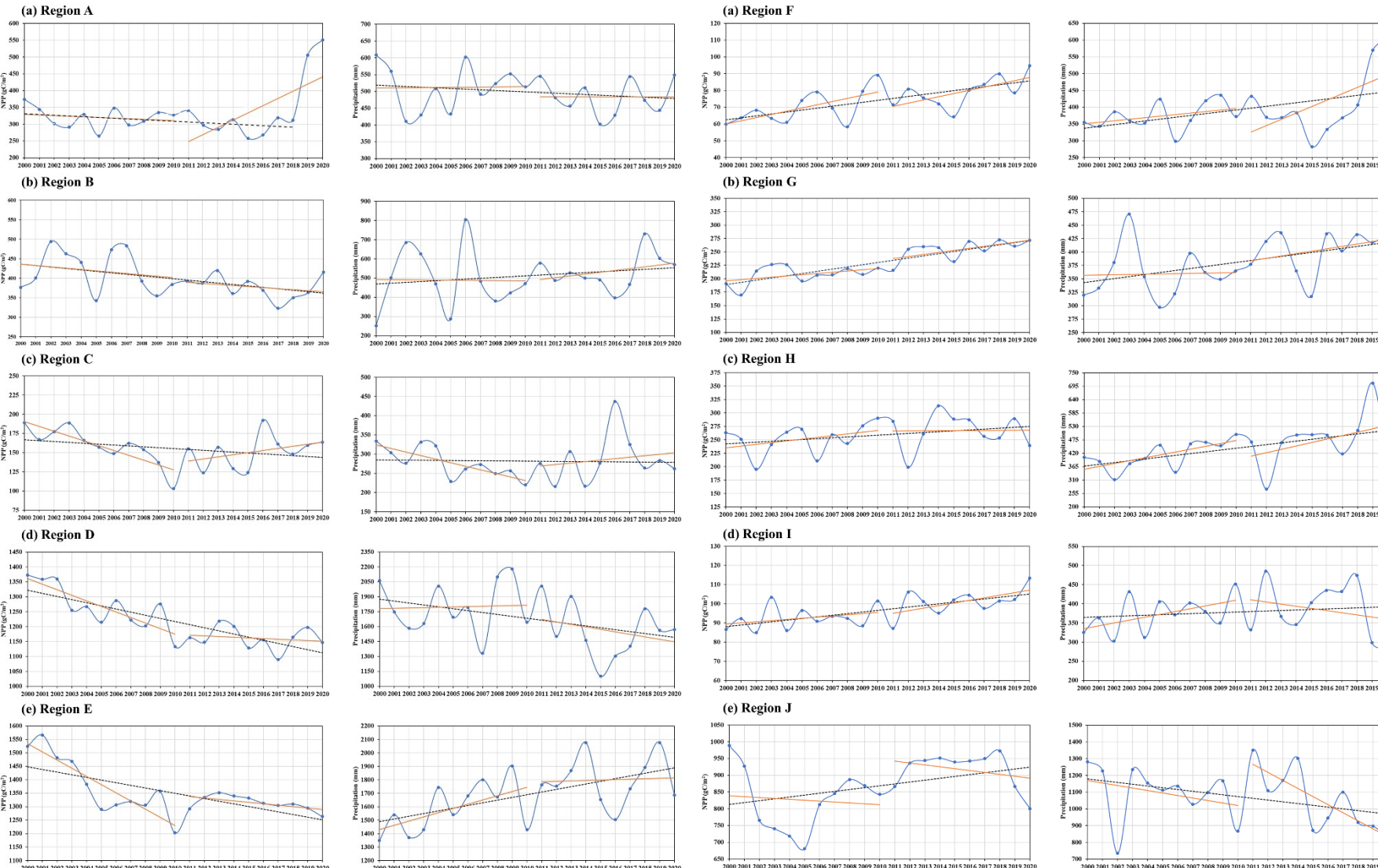
Distribution of global grassland degrading driving factors



Distribution of global grassland improving driving factors



Global grassland degrading (a) and improving (b) proportion of driving factors in different climatic regions



Precipitation and NPP variations in degrading grassland hotspots

Precipitation and NPP variations in improving grassland hotspots

(1) The trend of NPP and precipitation is the same, and the fluctuation of NPP was mainly controlled by precipitation.

(2) The overall trends of NPP and precipitation are consistent, but the segmental interannual variability or the degree of variation is not identical.

(3) The trends in NPP and precipitation are precisely opposite.

Discussion

- (1) Mapping global grassland degradation and improvement.
- (2) Irregular processes of global grassland degradation driven by climate change and human activities.
- (3) Implications in grassland degradation trends studies and future opportunities.

Conclusions

(1) Grassland degradation and improvement processes are happening globally, with an overall improvement trend. Improved grassland area is 1.92 times larger than degraded grassland. Semi-humid and humid regions experience the least degradation.

(2) Africa faces significant grassland degradation, while Asia leads in grassland improvement. However, the global land degradation crisis remains a serious obstacle to achieving Land Degradation Neutrality (LDN).

(3) Climate change and human activities are the main drivers of grassland degradation, accounting for 84.72% and 87.76% of the combined effects, respectively. Human activities have reversed degradation in some regions, but extensive cultivation and poor land management can worsen degradation.

(4) Priorities include long-term care of grassland degradation hotspots, targeted interventions, and sharing successful management experiences to address the global land degradation crisis and contribute to Sustainable Development Goal 15.3 for a land degradation-neutral world.

- Inform on the project's schedule, planning & contribution of the partners for the following year
 - validation of results
 - consultation with end users
 - final reporting & publishing

- Report on the level and training of young scientists on the project achievements, including plans for academic exchanges

Name	Institution	Poster title	Contribution including period of research
Li Changlong	Guangzhou College of Commerce	Characteristics of Vegetation Dynamic Changes in the Beijing-Tianjin Sandstorm Source Area in the Past 20 Years	Mapping and dynamic monitoring of grassland types
Cui Hanwen	IFRIT, CAF/AIR, CAS	Generation of Daily Mid-high Spatial Resolution Surface Reflectance Dataset and its Application in Grassland Utilization Intensity Monitoring	Quantitative estimation of grassland ecological

Two student from University of Leeds will visit CAS and CAF in the following year.

- Report on the peer reviewed publications (nr. of papers, journal name and publication title) after 3 years of activity
1. Bin Sun, Pengyao Qin, Changlong Li, et al. Integrating vegetation phenological characteristics and polarization features with object-oriented techniques for grassland type identification [J], Geo-spatial Information Science(accepted)
 2. Yan Ziyu, Gao Zhihai, Sun Bin, et al. Global degradation trends of grassland and their driving factors since 2000[J], International Journal of Digital Earth. 2023, 16(1), 1661-1684

Thanks for your attention

